Proceedings of the ASME 2010 3rd Joint US-European Fluids Engineering Summer Meeting and 8th International Conference on Nanochannels, Microchannels, and Minichannels
FEDSM-ICNMM2010
August 1-5, 2010, Montreal, Canada

FEDSM-ICNMM2010-30749

SUBMERGED JET IMPINGEMENT BOILING OF SATURATED WATER UNDER SUB-ATMOSPHERIC CONDITIONS

Ruander Cardenas
Oregon State University
204 Rogers Hall, Mechanical Engineering,
Corvallis, OR 97331-6001

Preeti Mani
Oregon State University
204 Rogers Hall, Mechanical Engineering,
Corvallis, OR 97331-6001

Vinod Narayanan[1]
Oregon State University
204 Rogers Hall, Mechanical Engineering,
Corvallis, OR 97331-6001
[1]vinod.narayanan@oregonstate.edu

ABSTRACT
An experimental study of mini-jet impingement boiling is presented for saturated conditions. Unique to this study is documentation of boiling characteristics of a submerged water jet under sub-atmospheric conditions. Data are reported at a fixed nozzle-to-surface distance that corresponds to a monotonic decrease in heat transfer coefficient for single-phase jet impingement. A mini nozzle is used in the present study with an internal diameter of 1.16 mm. Experiments are performed at three sub-atmospheric pool pressures of 0.2 bar, 0.3 bar and 0.5 bar. At each pressure, jet impingement boiling at four Reynolds numbers are characterized and compared with the pool boiling heat transfer. Enhancements in critical heat flux with increasing Re are observed for all pressures.

INTRODUCTION
Enhancement of single phase and phase change heat transfer using jet impingement has been studied for several decades. Applications as diverse as internal cooling of gas turbine blades, drying of textiles and food, and metals processing have benefitted from use of jet impingement heat transfer. The attraction of jet impingement lies in the high heat transfer coefficient at the impingement region, where the jet fluid is in direct contact with the surface. A boundary layer forms as the impinged fluid accelerates along the surface in an outward direction from the impingement point to form a wall jet. By placing multiple jets at appropriate locations in an array, it is possible to reap the benefits of periodic redevelopment of boundary layers and high heat transfer rates at impingement locations. Various configurations of nozzles and nozzle arrays have been developed over the past decades; some offer specific advantages over others for particular applications. For single-phase jet impingement heat transfer, the review papers by Martin [1] and Viskanta [2] provide the basics of hydrodynamics and heat transport and also serve as excellent compendia of work performed in the field.

The present work documents phase-change heat transfer, in particular, boiling, during jet impingement. Jet impingement boiling refers to a condition where a single-phase jet impinges on a hot surface and undergoes phase change at that surface. Numerous studies on jet impingement boiling on a heated surface exist in the context of metals processing, and more recently, electronics cooling. Wolf et al. [3] provide an exhaustive summary of work performed until 1993 in this field. Literature on four different types of liquid jet impingement boiling were summarized in their review paper, namely, (i) free surface liquid jets, (ii) submerged jets, (iii) plunging jets, and (iv) confined jets. Most of jet impingement boiling research has been performed on free surface liquid jets, wherein the liquid jet issues from the nozzle and is surrounded by a gaseous environment. In contrast, submerged jets refer to a condition where the jet issues into a fluid with the same environment as the jet. Plunging jets issue as a free surface jet, but enter a pool of liquid prior to impinging on the surface. Confined jets are a particular case of submerged jet wherein the liquid surrounding the nozzle is constrained by an upper wall.

Several similarities exist between the four jet configurations mentioned above as far as jet impingement boiling characteristics is concerned, such as insensitivity of the onset of nucleation to jet parameters and the invariance of the fully developed nucleate boiling curve from that of pool boiling. However, differences in heat transfer are to be expected with respect to nozzle-to-surface standoff distance and nozzle to heater diameter ratio. The effect of these two parameters on heat transfer is discussed below.

Submerged jet impingement is sensitive to nozzle-to-surface distance parameter due to entrainment of surrounding fluid. Mass entrainment of quiescent fluid causes a reduction in the potential core of the jet with downstream distance from the nozzle. Typically, the heat transfer surface is placed between 5 and 7 diameters, which is the downstream distance at which the potential core merges to form a stagnation point (or line). With further increase in nozzle-to-surface spacing, the momentum of the jet at the impingement location decreases and heat transfer rates are reduced as well. On the flip side, since the jet spread is larger, temperature gradients along the surface are generally smaller for submerged jet impingement. For boiling conditions, it is possible with submerged jet conditions for vapor bubbles to get entrained in the jet flow and be impinged on the surface. This entrapped vapor could potentially act as a nucleation site when lodged on the surface or it could slide along the surface and enhance heat transfer [4,5].

Wolf et al.'s literature review documents mainly two distinct conditions at the critical heat flux (CHF) condition. The first CHF condition comes to bear when the jet velocity is low or the surface area to jet area is large. Under either of these configurations, CHF is reached prematurely due to inability of the jet to rewet the surface effectively. In other words, the heat transfer rate from the surface, $q''_{CHF}A_s$, is greater than the latent heat capacity rate of the saturated jet, $\left(\rho_l V_j A_j\right) h_{lv}$. While this condition has been shown to exist in free-surface jets, there is little information on whether this condition would exist in submerged jet boiling. If it did exist, there remains a legitimate question of whether this condition would have different limits of jet velocity and diameter ratio than in free-surface jet boiling. In addition, droplet breakup and ejection are prone to occur in free-surface jets with thin liquid film coverage, resulting in premature CHF condition. The more common CHF condition is that of variation of CHF with jet velocity, which occurs when the heat transfer rate from the surface is only a small fraction of the jet latent heat capacity rate.

Despite the vast interest in jet impingement boiling, surprisingly little work has been performed in submerged environment. Katto and Kunihiro [6] were among the first to document the differences between free surface and submerged jet impingement configurations. In an attempt to enhance critical heat flux using water as the working fluid, they studied, under saturated conditions, different pool heights and nozzle-to-surface distance for jet velocities that ranged from 2.04 - 2.64 m/s. They observed that there was no difference in the nucleate boiling curve between pool boiling and jet impingement boiling. The above conclusion has since been reiterated by several investigators [3]. A salient conclusion was that submerged jet impingement boiling resulted in an increased CHF, by as much as 25 percent at 3 m/s compared with free surface jet impingement boiling. This enhancement in CHF was found to increase with jet velocity.

Ma and Bergles [7] documented the incipience of nucleate boiling and fully developed nucleate boiling for R-113 jet impingement boiling. Like Kunihiro and Katto [6], they too found that jet velocity did not have any effect of the fully developed nucleate boiling curve and that subcooling shifted the curve to the left slightly. They provided correlations for predicting the onset of boiling and for the partial boiling regime. Despite regular cleaning and degassing procedures, the boiling curves were found to change with experimental runs. Zhou et al. [8] and Zhou and Ma [9] also presented data on R-113 jet impingement boiling. They noticed similar trends to that of Ma and Bergles [7]. Higher CHF was obtained and was attributed to the smaller surface to nozzle diameter ratio. They also presented a correction to the saturation temperature based on the stagnation pressure of the jet for high jet velocities (>10 m/s in their study).

In jet impingement boiling, nucleation is initiated at the periphery of the heated surface that is farthest away from the jet influence and proceeds inward with an increase in heat flux. Dukle and Hollingsworth [10,11] vividly portray the boiling front for nozzle-to-surface distances of 8.2 [10], for which a monotonic heat transfer distribution occurs, and for a distance of 2.3 [11], for which a secondary peak in heat transfer occurs. Using liquid crystal imaging, they were able to locate the areas of single-phase jet convection and nucleate boiling, and thereby, to identify the boiling front. They noted that for the larger nozzle spacing, at any particular heat flux preceding complete nucleate boiling on the surface, the boiling front was stabilized by the large surface temperature gradients produced by the jet flow. In contrast, the non-monotonic surface temperature distribution set up at closer spacings resulted in a collapse of the boiling front in the region of the secondary peak in surface temperature. The salient conclusion of their work is that the radially-averaged boiling front location in the wall jet region can be predicted by single-phase heat transfer distribution.

In summary, global experiments in conjunction with a few imaging experiments have identified and described the process of nucleation onset and partial nucleate boiling regimes in submerged jet impingement. Critical heat flux data for R-113 have also been quantified over a sufficiently wide range of jet velocities. However, significant gap exists in literature on jet impingement boiling with water. To the best of the authors' knowledge, no work exists on sub-atmospheric submerged jet impingement boiling.

OBJECTIVES

This paper presents submerged jet impingement boiling of water at sub-atmospheric conditions. The work is inspired by the practical application of thermal management of electronics that normally need to be maintained at temperatures below 85 ^{o}C. Typically dielectric fluids are used to cool such electronic devices. However, water has superior thermal properties (high thermal conductivity, specific heat and specific enthalpy of vaporization) and is hence the fluid of choice for high-flux cooling applications. Recently, Pal et al. [12] reported improved performance of a thermosyphon that operated with a sub-atmospheric evaporator pressure using deionized water compared with a thermosyphon that used dielectric fluid PF5050. In order to apply jet impingement boiling using water to high flux electronics cooling, it is similarly necessary to perform experiments at sub-atmospheric pressures.

Jet impingement boiling experiments were performed at three sub-atmospheric pressures of 0.2, 0.3, and 0.5 bar. At each pressure, the jet Reynolds number was varied. The corresponding density ratio, ρ_L/ρ_v are between 1.9 – 4.6 times larger than at atmospheric pressure. Experiments were performed at a fixed non-dimensional nozzle-to-surface distance H/d_j of 6 corresponding with a monotonic decay in heat transfer coefficient profile, and for one surface-to-nozzle diameter ratio of 23.8.

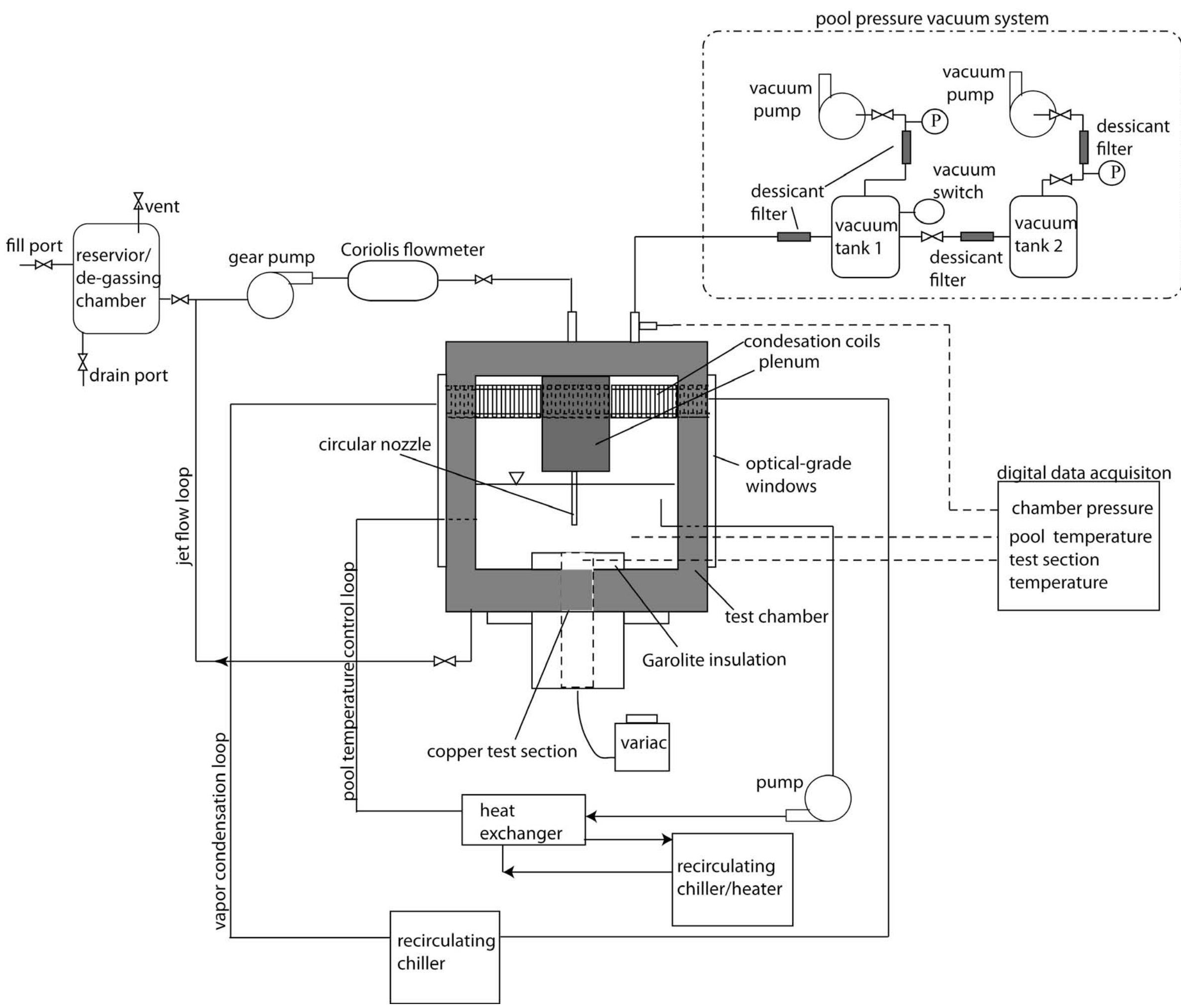

Fig.1. Schematic of the experimental facility

NOMENCLATURE

C_p specific heat at constant pressure (J/kg-K)
d diameter (m)
Gr Grashof number ($Gr = g\beta d_s^3 (T_s - T_\infty)/\upsilon^2$)
H nozzle standoff distance from the surface (m)
h_{fg} specific enthalpy of vaporization (J/kg)
k thermal conductivity of copper (W/m-K)
Nu Nusselt number ($Nu = hd_s/k_f$)
P pressure (Pa)
Pr Prandtl number ($Pr = \upsilon/\alpha$)
q'' heat flux (W/cm^2)
Ra Rayleigh number (Gr.Pr)
Re Reynolds number ($Re = \rho V d/\mu$)
T temperature (^{o}C)
V velocity (m/s)

Subscripts
ch chamber
CHF critical heat flux
F fluid
j jet
l liquid
s surface
sat saturation
v vapor

Symbols
α thermal diffusivity (m^2/s)
β temperature coefficient of expansion (K^{-1})
μ dynamic viscosity
ν kinematic viscosity (m^2/s)
ρ density (kg/m^3)
σ surface tension (N/m)

EXPERIMENTAL FACILITY AND TEST SECTION

Figure 1 provides a simplified schematic of the experimental facility for sub-atmospheric jet impingement boiling. It consists of a central test chamber and five sub-systems: (a) pool subcooling loop, (b) pool vapor condensation loop, (c) pool pressure control sub-system, (d) test section, and (e) data acquisition sub-system. The test chamber has high-transmissivity glass windows on three faces to permit quantitative flow visualization in future studies. For purposes of global measurements presented in this paper, the glass windows are replaced with clear polycarbonate windows. Pool pressure is maintained using a vacuum sub-system as illustrated in Fig. 1. It consists of two vacuum tanks connected in line and two vacuum pumps. The lines have desiccant filters at several locations to protect the tanks and pumps. A calibrated digital pressure transducer records the pool pressure. A valve in the vacuum line is used to regulate the pool pressure from 0.05 bar to 1 bar. This sub-system is able to provide variable, stable pool pressures through the duration of an experiment (~10-12 hours).

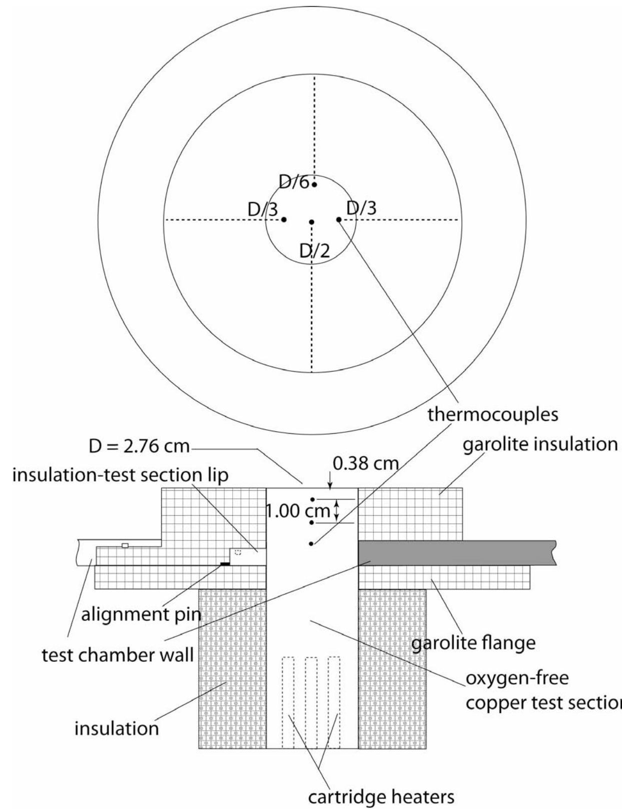

Fig. 2. Schematic of the test section

The jet flow loop consists of a variable-speed gear pump (Micropump) that supplies deionized, degassed water to the jet plenum chamber in the test section (see Fig. 1). A Coriolis flowmeter (Micromotion Elite II) monitors the jet mass flow rate and density. Variable diameter and length nozzles can be affixed at the end of the jet plenum chamber. The flow exits the nozzle as a circular jet that impinges on the heated test section.
The test section is shown schematically in Fig. 2. It consists of an oxygen-free copper cylinder that is heated from below using five 250-watt cartridge heaters. A variable transformer supplies power to the cartridge heaters. The sides of the copper test section are thoroughly insulated with garolite on the upper part and with high-temperature insulation on the bottom part in order to minimize heat losses and thereby ensure heat conduction along the copper rod. Three thermocouples are located along the axis on the upper part of the copper test section and are used to determine the heat flux based on a one-dimension heat conduction model. The top thermocouple is 0.38 cm away from the surface and is used to determine the surface temperature. Three other thermocouples are located at different peripheral distances at this depth from the top surface as shown in Fig. 2. These thermocouples were located with the intention of determining radial variations in near-surface temperature during the jet impingement boiling process. The copper test section has a lip with an o-ring that provides a seal between the test section and garolite insulation. A garolite flange holds the test section in place at the bottom of the test chamber as shown in Fig. 2. An o-ring, located on the bottom

face of the test chamber, provides a seal between the copper test section and the test chamber.

Pool subcooling is maintained using a sub-loop that consists of a pump and a heat exchanger. A ThermoHaake recirculating heater/chiller provides the necessary heating/cooling to the heat exchanger. Pool temperature is monitored at three locations within the liquid in the chamber. Condensation coils are located at the top corner of the test section. A Thermo Scientific recirculating chiller provides fluid at the required temperature. Temperatures in the copper test section and pool, along with the pool pressure, are monitored using a digital data acquisition system (National Instruments) using a LabVIEW program. Thermocouples are calibrated using a NIST-traceable RTD and the sub-atmospheric pressures are calibrated using a precision analog gage.

EXPERIMENTAL PROCEDURE

Experiments on sub-atmospheric pool boiling with water as the working fluid were performed at three pool pressures and for four jet Reynolds numbers. Saturated conditions were maintained at each pool pressure for these experiments. The jet impingement boiling data were compared against a reference pool boiling condition at the corresponding pressure.

A 1.16 mm inner diameter nozzle was used for the experiments. It was located centrally above the copper test section. The diameter of the surface to that of the nozzle, d_s/d_j was 23.8, and the corresponding area ratio was 566.3. As a reference, d_s/d_j in the study of Katto and Kunihiro [6] varied from 6.25-14. Their study also made use of a copper surface with axial thermocouples used for heat flux determination. The d_s/d_j ratio becomes a significant parameter in determining CHF, especially for free surface jet impingement boiling. Prior to an experimental run at each pressure, the copper surface was sanded with a 600 grit emery paper and washed with acetone and deionized water.

The nozzle-to-surface spacing (standoff distance) was kept constant at 6. This spacing corresponds to the maximum heat transfer at the stagnation point in single-phase submerged jet impingement literature [1,2]. For this nozzle-to-surface distance, the radial distribution of heat transfer coefficient decreases monotonically from the impingement point outward.

Table 1. Estimate of uncertainty

Variable	Uncertainty
Thermocouples used for heat flux (°C)	±0.57
Heat flux (W/cm²)	1.5
Critical heat flux (percent)	3
Surface temperature estimate (°C)	±0.7
Excess temperature estimate (°C)	± 0.75

The nozzle height above the surface was determined through visual images of the nozzle alongside a calibrated grid. These images were captured using a CCD camera. De-ionized, degassed water was used as the testing fluid. Using the vacuum tanks the chamber pressure was adjusted to the required value, and monitored by a pressure transducer. The pool was heated using the Thermohaake circulator to the required saturation temperature. The pool was initially mixed using the jet to ensure a uniform temperature. Data collection was started once steady state was attained. Staring at zero power, the heat input to the Cu surface was incremented in steps of three percent after the pool attained a steady state. This was continued all the way till CHF was attained at which point the heat input to the surface was turned off.

DATA ANALYSIS

Heat flux was calculated from three temperature measurements collected axially using a 1-D steady heat conduction model. The conductivity used in the model was evaluated at the average temperature between the two end temperatures. Three different values of heat flux were calculated from the temperature values and their corresponding spacings. The different values of heat flux were within 0.1 percent of each other in the nucleate boiling regime. The reported heat flux value corresponds to the average of the three heat flux values calculated from this method.

The thermocouple closest to the surface was located 3.81 mm below the surface. The estimated heat flux value was used together with a 1-D conduction model to determine the temperature of the surface. At high heat flux values, the surface temperature is significantly lower than the temperature

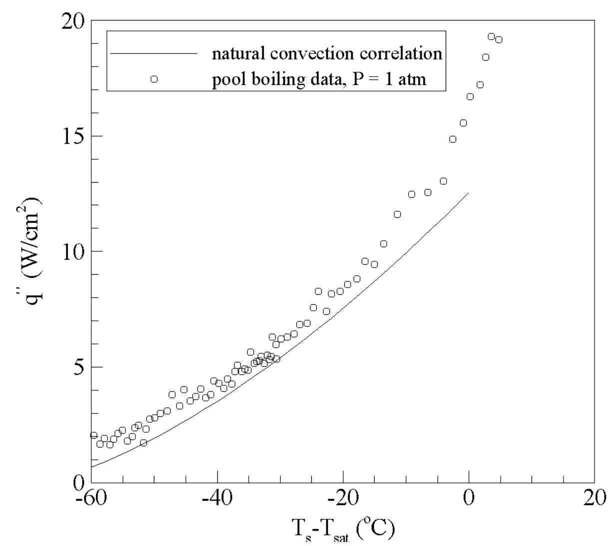

Fig. 3. Comparison of single-phase data with correlation (Eq. 1)

measured 3.81 mm beneath the surface despite the high thermal conductivity of copper. The saturation temperature needed to compute the surface super heat was found from the averaged pressure measured through the duration of each experiment. All fluid properties were evaluated at the measured temperature and pressure utilizing the routines in Engineering Equation Solver (EES) software. An uncertainty analysis was performed on the measured and determined global variables and is reported in Table 1. The Kline and McKlintock method [13] was used to propagate errors from measured to calculated variables.

RESULTS AND DISCUSSION

Preliminary validation experiments were performed to benchmark single-phase natural convection and pool boiling against standard correlations in the literature. Figure 3 shows a plot of heat flux as a function of wall superheat in the single-phase region for a highly sub-cooled condition at atmospheric pressure. This data is compared against a standard natural convective correlation for heated horizontal surface facing up [14]

$$\overline{Nu_{d_s}} = 0.54 Ra_{d_s}^{1/4} \qquad [1]$$

This correlation is valid for a range of Rayleigh numbers from 10^4 to 10^7. Considerably good agreement (within 10 percent) is observed between the correlation and the experimental data up to a heat flux of about 10 W/cm^2.

Next, the nucleate boiling data from the same experimental run was compared against the Rohsenow correlation [14],

$$q''_s = \mu_l h_{fg}\left[\frac{g(\rho_l-\rho_v)}{\sigma}\right]^{1/2}\left(\frac{C_{p,l}[T_s-T_{sat}]}{C_{s,f} h_{fg}\, Pr_l^n}\right)^3 \qquad [2]$$

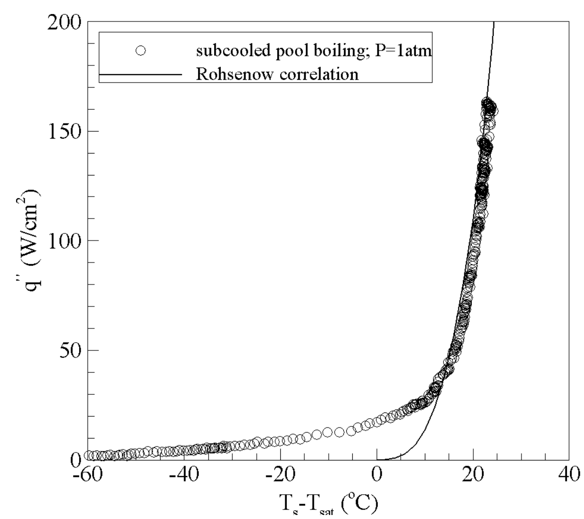

Fig. 4. Comparison of nucleate boiling data with Rohsenow correlation at atmospheric pressure.

A $C_{s,f}$ value 0.0128 for water on polished copper surface and a Prandtl number exponent of unity were used in the correlation. The nucleate boiling data shown in Fig. 4 was found to be in good agreement with the Rohsenow correlation. In general, the correlation predicts a slightly higher heat flux for a given superheat, but the data are within experimental uncertainty of the correlation.

To provide a reference condition for comparison of jet impingement data, pool boiling experiments were performed at different pressures. Figure 5 presents the pool boiling data at pressures of 0.08, 0.2, 0.3, and 0.5 bar. As expected, an

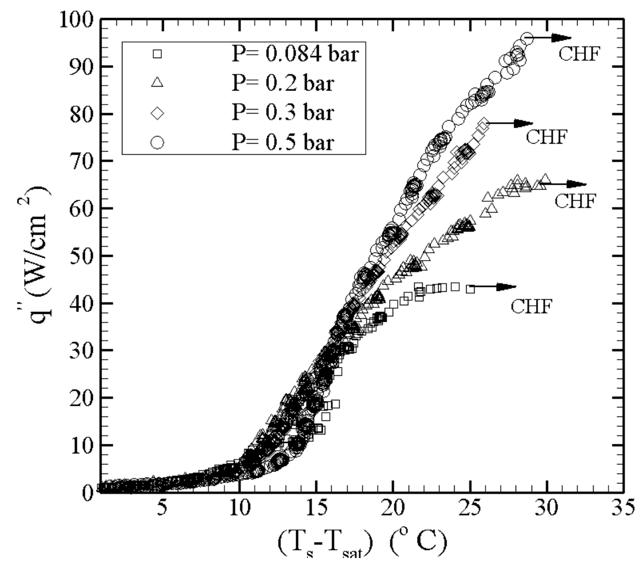

Fig. 5. Pool boiling curves at various sub-atmospheric pressures

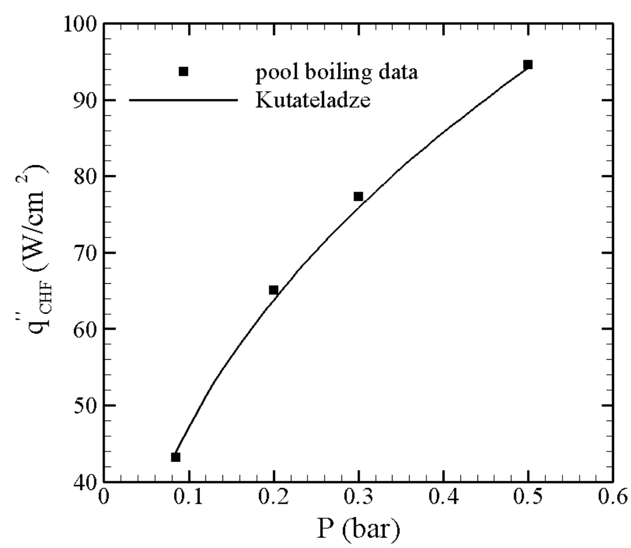

Fig. 6. Comparison of pool boiling critical heat flux with Kutateladze's correlation

Table 2. Experimental Matrix and critical heat flux data

Chamber Pressure P_{ch} (bar), Saturation Temperature ($T_{ch,sat}$)	Jet Exit Velocity V_j (m/s)	Jet Reynolds Number, Re_j	q''_{CHF} (W/cm^2)
0.2 (60 °C)	0*	0	65
	0.81	1830	71
	1.58	3573	82
	2.43	5510	94
	3.86	8844	118
0.3 (69.1 °C)	0*	0	77
	0.75	1968	89
	2.20	5731	116
	3.48	9168	143
	4.90	12791	176
0.5 (81.3 °C)	0*	0	95
	0.61	1853	105
	1.83	5472	134
	3.04	9105	162
	4.18	12634	191**

* pool boiling **near CHF limited by heater power

increase in critical heat flux is observed with increasing pressure. Figure 6 presents the critical heat flux data for pool boiling under these pressures indicating this trend. Also plotted is a trend line of CHF prediction using Kutateladze's correlation [14],

$$q''_{max,sat} = Ch_{fg}\rho_v\left[\frac{\sigma g(\rho_l - \rho_v)}{\rho_v^2}\right]^{1/4} \qquad [3]$$

A C value of 0.149, corresponding to a large horizontal heated plate is used in this correlation. Despite the changes in pressure, a very good agreement between this correlation and experimental data is observed. Although pressure is not directly included in the correlation, its effect is implicitly captured by the change in vapor density, $q''_{max,sat} \propto \rho_v^{1/2}$.

Table 2 summarizes the experimental matrix including saturation temperature, jet velocity, and jet Reynolds number. Jet impingement boiling experiments were performed at absolute pressures of 0.2, 0.3, and 0.5 bar. Reference pool boiling data was collected at these pressures as well as at a lower pressure of 0.08 bar (see Fig. 5). Jet impingement data at the low pool pressure of 0.08 bar could not be collected due to the limitation of the pump. Also provided in Table 2 are CHF values for the experimental conditions for which results are shown. Jet exit velocities in the range of 0.6-4.9 m/s were tested; the pump placed the higher limit on velocity in the

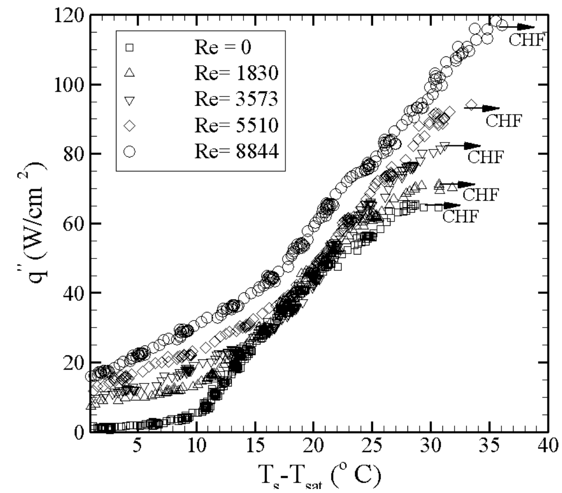

Fig. 7. Jet impingement boiling curves at P=0.2 bar

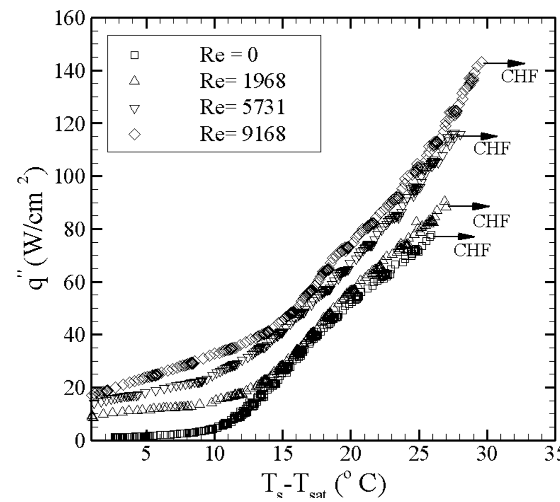

Fig. 8. Jet impingement boiling curves at P= 0.3 bar

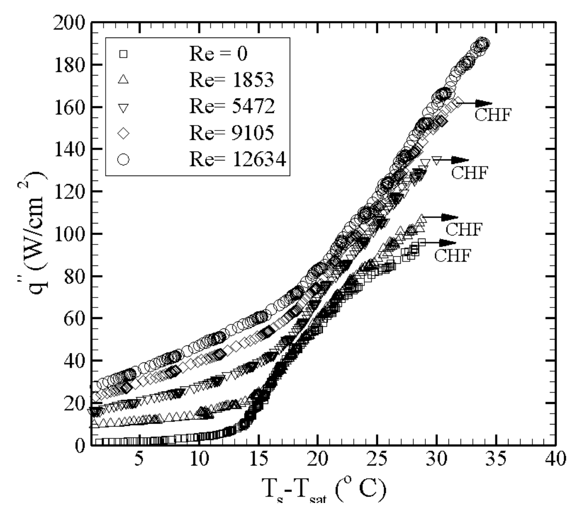

Fig. 9. Jet impingement boiling curves at P= 0.5 bar

experiments. As a reference, Katto and Kunihiro's [6] study had a V_j range of 2.04-2.64 m/s. All boiling curves were recorded under increasing heat flux conditions. Critical heat flux for the P = 0.5 bar and Re = 12634 was not attained owing to heater power limitations. However, visual observations indicated that the boiling condition on the surface was close to that seen at CHF.

Figures 7-9 present boiling curves at P = 0.2, 0.3, and 0.5 bar, respectively. A common trend in all plots is that in the single-phase region, jet flow enhances the area-averaged heat transfer rate from the surface, as evident from the increase in the slope of the curves with jet impingement. Also as expected, a higher Reynolds number jet flow results in a higher single-phase heat transfer coefficient. No incipience temperature overshoot is observed in any of the boiling curves.

Visual observations indicated that at the onset of boiling for jet impingement, boiling front progresses from the periphery of the copper surface towards the center and upon application of a sufficiently high heat flux, boiling occurs over the entire surface. This progressive boiling front, which is clearly visible for the higher Re jet at all pool pressures, results in a less pronounced "knee" of the boiling curve. One interesting point to consider is the increase in pressure for the high Re jet. Zhou and Ma [9] incorporated a correction for the increase in stagnation pressure (and hence saturation temperature) in terms of a subcooling effect. This correction tends to shift the boiling curve for the high velocity jets to the left. Although they observed that the sub-cooling correction is significant for velocities in excess of 10 m/s, since the present experiments are performed at sub-atmospheric conditions, a lower velocity could significantly impact the rise in saturation temperature. As an example, for the Re = 8870 jet, rise in stagnation pressure is of the order of 11.97 kPa, corresponding to a 33 percent increase in pressure. However, taking into consideration that

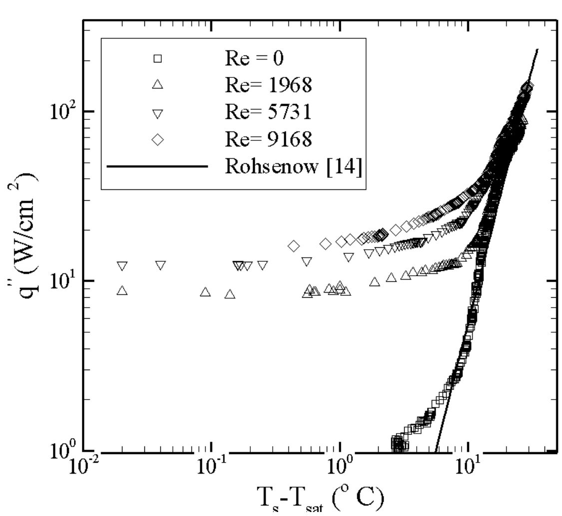

Fig. 10. Comparison of Rohsenow correlation [14] with jet impingement and pool boiling data

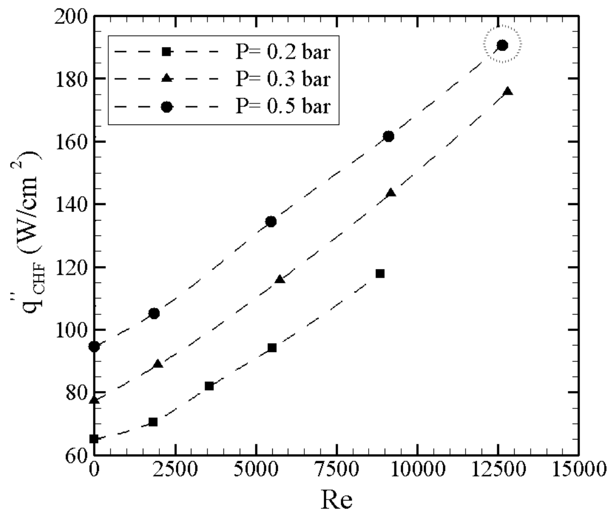

Fig. 11. Critical heat flux data for conditions summarized in Table 2.

this increase is experienced over a very small region of the surface (owing to the large d_s/d_j ratio as well as reduction in momentum prior to impingement), no correction was deemed necessary or appropriate.

In order to further clarify the trend in the fully developed nucleate boiling regime, data for P = 0.3 bar in Fig. 8 is re-plotted on a log-log scale in Fig. 10. Also provided for comparison in this figure is Rohsenow's correlation, Eq. 2. The independence of heat flux on excess temperature in the single-phase region is evident from the figure. This trend should be expected since heat transfer rate in this region is governed only by the hydrodynamics of jet impingement for a given fluid. Larger Reynolds number jets have a more pronounced partial nucleate boiling regime compared with the pool boiling or low Reynolds number jet conditions. Note also that the fully developed nucleate boiling region of the curve is over a smaller extent at these higher Re. However, irrespective of the Re, the fully developed nucleate boiling part of the boiling curve is fairly independent of the velocity. This invariance of boiling curve with jet velocity has been reiterated in literature on free surface as well as submerged jet impingement [3].

The CHF data from Figs. 7-9 are shown in Fig. 11. As mentioned before, at P=0.5 bar and the highest Re (see circled datapoint), CHF was not achieved; however visual observations had indicated that it was imminent. Hence, this datapoint has been included in Fig. 11. At each pressure, an increase in CHF with Re is evident. Increase in CHF in excess of 70 percent are seen for a modest jet Re of ~9000.

As mentioned in the introduction section, for free surface jets, a lower latent heat capacity rate of the jet when compared with the CHF heat transfer rate is indicative of premature CHF due to dryout. For free surface jets, it is possible to obtain lower

CHF than for pool boiling in such operating conditions. For submerged jets, since a pool surrounds the surface, the worst-case CHF reverts back to that of pool boiling. Calculations show that the jet latent heat capacity rate, despite the low jet velocities, ranges from 2.3 to 13.4 times that of the CHF heat transfer rate, due to the large enthalpy of vaporization of water. Hence, an increase in CHF should be expected, and is seen, for even low Re jet impingement.

CONCLUSIONS

Saturated jet impingement boiling experiments were performed at sub-atmospheric pressures using water as the working fluid. The nozzle-to-surface spacing was kept constant at 6 nozzle diameters and the surface-to-nozzle diameter was held constant at 23.8. Sub-atmospheric pool boiling critical heat flux data is well predicted by the Kutateladze correlation. Results of jet impingement boiling indicate that critical heat flux increases with jet exit Re at all three pressures studied. Enhancements in excess of 70 percent for jet Re of 9000 are seen for all pressures.

ACKNOWLEDGMENTS

Financial support for this project is provided by the National Science Foundation under award number 0748249.

REFERENCES

1. Martin, H., 1977, “Heat and Mass Transfer between Impinging Gas Jets and Solid Surfaces,” Advances in Heat Transfer, **13**, pp. 1-60.
2. R. Viskanta, 1993, “Heat Transfer to Impinging Isothermal Gas and Flame Jets,” Experimental Thermal and Fluid Science, **6**, pp. 111-134.
3. Wolf, D. H., Incropera, F. P., and Viskanta, R., 1993, “Jet Impingement Boiling,” Advances in Heat Transfer, **23**, pp. 1-132.
4. Bayazit, B. B., Hollingsworth, D. K., and Witte, L. C., 2003, “Heat Transfer Enhancement Caused by Sliding Bubbles,” Journal of Heat Transfer, **125**, pp. 503 - 509.
5. Thorncroft, G. E., and Klausner, J. E., 1999, “The Influence of Vapor Bubble Sliding on Forced Convection Boiling Heat Transfer,” Journal of Heat Transfer, **121**, pp. 73-79.
6. Katto, Y., and Kunihiro, M., 1973, “Study of the Mechanism of Burn-out in Boiling System of High Burn-out Heat Flux,” Bulletin of the Japanese Society of Mechanical Engineers, **16** (99), pp. 1357-1366.
7. Ma, C. F., and Bergles, A. E., 1986, “Jet Impingement Nucleate Boiling,” International Journal of Heat and Mass Transfer, **29** (8), pp. 1095-1101.
8. Zhou, D. W., Ma, C. F., Yu, J., 2004, “Boiling hysteresis of impinging circular submerged jets with highly wetting liquids,” International Journal of Heat and Fluid Flow, **25**, pp. 81-90.
9. Zhou, D. W., Ma, C. F., 2004, “Local jet impingement boiling heat transfer with R113,” Heat and Mass Transfer, **40**, pp. 539-549.
10. Dukle, N. M., Hollingsworth, D. K., 1996, “Liquid Crystal Images of the Transition from Jet Impingement Convection to Nucleate Boiling Part I: Monotonic Distribution of the Convection Coefficient,” Experimental Thermal and Fluid Science, **12**, pp. 274-287.
11. Dukle, N. M., Hollingsworth, D. K., 1996, “Liquid Crystal Images of the Transition from Jet Impingement Convection to Nucleate Boiling Part II: Nonmonotonic Distribution of the Convection Coefficient,” Experimental Thermal and Fluid Science, **12**, pp. 288-297.
12. Pal, A., Joshi, Y., Bietelmal, M. H., Patel, C. D., and Wenger, T. M., 2002, “Design and Performance Evaluation of a Compact Thermosyphon,” IEEE Transactions on Components and Packaging Technologies, **25** (4), pp. 601-607.
13. Moffat, R. J., 1988, “Describing Uncertainties in Experimental Results*,” Experimental Thermal and Fluid Science*, **1**, pp. 3-17.
14. Incropera, F. P., DeWitt, D. P., Bergman, T. L., Lavine, A. S., 2006, *Fundamentals of Heat and Mass Transfer,* Sixth Ed., John Wiley & Sons, NY.